Atmos. Chem. Phys. Discuss., 12, 12119–12162, 2012
www.atmos-chem-phys-discuss.net/12/12119/2012/
doi:10.5194/acpd-12-12119-2012

Atmospheric Chemistry and Physics Discussions

Observation of aerosol size distribution and new particle formation at a mountain site in subtropical Hong Kong

H. Guo[1], D. W. Wang[1], Z. H. Ling[1], C. K. Chan[2], and X. H. Yao[3]

[1]Air Quality Studies, Department of Civil and Structural Engineering, The Hong Kong Polytechnic University, Hong Kong, China
[2]Division of Environment and Department of Chemical and Biomolecular Engineering, The Hong Kong University of Science and Technology, Hong Kong, China
[3]Key Lab of Marine Environmental Science and Ecology, Ministry of Education, Ocean University of China, Qingdao, China

Received: 28 March 2012 – Accepted: 22 April 2012 – Published: 10 May 2012

Correspondence to: H. Guo (ceguohai@polyu.edu.hk)

Published by Copernicus Publications on behalf of the European Geosciences Union.

Abstract

In order to investigate the atmospheric particle formation and growth processes, and to quantify the particle number (PN) concentration and size distributions in Hong Kong, a three-month intensive field measurement was conducted from September to November in 2010 near the mountain summit of Tai Mo Shan, a suburban site approximately the geographical centre of the New Territories in Hong Kong. The mean total number concentration in the size range of 5.5–350 nm was $7.86 \pm 0.66 \times 10^3\,cm^{-3}$ (mean ± 95% confidence interval), with a maximum value in November. New particle formation (NPF) events were observed on 12 out of 35 days in October/November 2010 with the formation rate from 0.29 to $4.53\,cm^{-3}\,s^{-1}$, and the average growth rates from 1.53 to $9.44\,nm\,h^{-1}$. The events usually began at 10:00 ~ 11:00 local time characterized by the occurrence of a nucleation mode with a peak diameter of 6 ~ 10 nm. The observed linear or non-linear correlations between nucleation mode PN concentration (5.5–10 nm) and ozone, volatile organic compounds (VOCs) and/or ($UV \times SO_2$) suggested critical roles of sulfuric acid and biogenic VOCs (e.g. isoprene, α-pinene and β-pinene) in the NPF events.

1 Introduction

Over the past decades, atmospheric submicrometer aerosols (< 1 μm in diameter) have been found to impact global climate (e.g., Twomey et al., 1984), air quality (USEPA, 1996), visibility (e.g., Mohan and Payra, 2009) and human health (e.g., Oberdorster et al., 2005). Typically, the sizes of submicrometer particles are categorized into three modes: a nucleation mode, representing quite newly formed particles usually have diameters smaller than 10 nm; Aitken and accumulation modes, representing aged particles generally ranged in size from 10 to 100 nm and from 100 to 1000 nm, respectively (e.g., McMurry et al., 2000; Seinfeld and Pandis, 2006). Especially, as the newly formed particles, parts of them can grow into cloud condensation nuclei (CCN) sizes,

ACPD
12, 12119–12162, 2012

significantly increasing the indirect radioactive effect of cloud (e.g., McMurry et al., 2011). Moreover, due to their nanometer-scale size, the newly formed particles can enter deep into the ciliated and alveolar sections of the lung and even bloodstream (Oberdorster et al., 2005), contributing to negative health effects. Consequently, it is critical to understand formation and growth processes of these new particles in the atmosphere.

To date, numerous measurements have been conducted in different locations to study the size distribution of submicrometer particles and new particle formation (NPF) processes, including free troposphere (e.g., Weber et al., 2001), boreal forests (e.g., Vehkamäki et al., 2004; Dal Maso et al., 2007; Asmi et al., 2011), coastal rural areas (e.g., Lee et al., 2008), high mountain-top (e.g., Gannet et al., 2011) and Antarctic/Arctic areas (e.g., Park et al., 2004). In addition, an increased number of studies were conducted in continental and coastal urban areas, i.e. Atlanta (Woo et al., 2001), St. Louis (Shi et al., 2002), East St. Louis (Qian et al., 2007), Pittsburgh (Stanier et al., 2004a,b), Birmingham, UK (Alam et al., 2003), Mexico City (Dunn et al., 2004), and Brisbane (Guo et al., 2008; Cheung et al., 2011). In China, the field measurements for particle size distribution were also carried out in several cities and regions in recent years. Short-term intensive studies on NPF were performed in Beijing (Yue et al., 2009), Pearl River Delta (PRD) (Liu et al., 2008), Yangtze River Delta (YRD) (Gao et al., 2009) and Hong Kong (Yao et al., 2010). Moreover, a couple of long-term continuous measurements were conducted in Beijing (e.g., Wu et al., 2008; Shen et al., 2011) and a remote mountain site, Mt. Waliguan (Kivekäs et al., 2009). Generally, nucleation events are much more frequently observed in rural/remote areas than in urban locations.

The production of atmospheric particulate matters normally requires two processes: the nucleation of stable atmospheric clusters (1–3 nm) and the growth of these clusters into observable sizes (> 3 nm) (Kulmala et al., 2000). In the first step of NPF, three classical nucleation theories are assumed to induce most NPF: (i) binary nucleation of sulfuric acid and water (H_2SO_4–H_2O); (ii) ternary nucleation involving a third molecule,

ACPD
12, 12119–12162, 2012

i.e. ammonia (NH_3) (H_2SO_4–H_2O–NH_3) and (iii) ion-induced nucleation. While the exact mechanisms and compounds participating in atmospheric NPF have remained unsolved. Recent studies (e.g., Kerminen et al., 2010) found that (i) nucleation is driven by sulfuric acid and possibly other low-volatile vapors (e.g. organics), and there was no indication from field measurements that water vapor participates into the nucleation; (ii) dimethylamine enhances the nucleation more effectively than ammonia in the atmosphere; and (iii) some organic acids produced from monoterpene oxidation can nucleate with sulfuric acid to form very stable clusters. The second step of particle growth is controlled by the competition between particle growth via complex mechanisms, and scavenging on the larger pre-existing particles (Kerminen et al., 2004). Actually, particle growth probably occurs due to the condensable vapors such as low VOCs. Both theoretical and experimental evidences suggest that a large number of charged and neutral clusters are almost always present in the atmosphere (Kulmala et al., 2007). Thus, the second step may be the limiting step in the atmospheric NPF.

Hong Kong is a coastal city located in the PRD region with a total land area of 1104 km^2 and a population of 7 million. Due to Hong Kong's special geographical location and complex atmospheric conditions, both local emissions and regional transport influence the Hong Kong's air quality. Previous studies indicate that air pollution caused by fine particulate matters and ozone (O_3) in the atmosphere of Hong Kong is severe (e.g., Wang et al., 2005; Guo et al., 2009a). It is well-known that both biogenic and anthropogenic VOCs together with nitrogen oxides (NO_x) are important precursors of surface-level O_3, and the oxidation products of photochemical reaction may play a key role in determining the spatial and temporal features of the nucleation events. Hence, NPF events likely occur along with photochemical O_3 production. To our best knowledge, only one study was conducted on atmospheric new particle growth and shrinkage at a coastal site in Hong Kong (Yao et al., 2010). No study on the characteristics of NPF events initiated or influenced by atmospheric photochemistry has been undertaken in Hong Kong so far. Therefore, it is urgent to enrich the database of particle number

ACPD
12, 12119–12162, 2012

(PN) concentration and size distribution, and to investigate the NPF processes in Hong Kong.

In this study, an intensive field measurement was conducted from 6 September to 30 November in 2010 near the summit of Mt. Tai Mo Shan (TMS; 640 m a.s.l). The PN concentration and size distribution were characterized and the NPF events were classified based on their strength and growth of geometric mean diameter (GMD). Moreover, the favorable meteorological conditions and possible mechanisms for the nucleation and growth of new particles were discussed by analyzing concurrently-observed meteorological parameters, gaseous pollutants, major hydrocarbons (e.g. isoprene, α- and β-pinenes, myrcene, limonene, toluene and $m/p/o$-xylenes), intermediate products i.e. methacrolein (MAC) and methyl vinyl ketone (MVK) generated from isoprene oxidation, carbonyl compounds i.e. formaldehyde, acetaldehyde and acetone, and 24–48 h $PM_{2.5}$ data.

2 Methodology

2.1 The topography and climate of Hong Kong

Hong Kong (22°15 N, 114°10 E) is surrounded by the South China Sea on the east, south, and west, and borders the Guangdong city of Shenzhen to the north over the Shenzhen River. The territory's 1104 km^2 area consists of Hong Kong Island, the Kowloon Peninsula, the New Territories, and over 200 offshore islands, of which the largest is Lantau Island where a power plant is located. The highest elevation in the territory is at TMS (957 m a.s.l.).

Hong Kong climate can be affected by severe weather phenomena including tropical cyclones, strong winter monsoon, and thunderstorms with associated squalls that are most frequent from April to September. Generally the dry monsoon season begins in mid to late September and brings three months of pleasantly warm days and clean air

ACPD
12, 12119–12162, 2012

masses. Hence, we chose these three months (September, October and November) as a sampling period for field measurement at TMS.

2.2 The sampling site

Mt. TMS is claimed to be Hong Kong's most misty area due to high daily clouds coverage. The highest point on Mt. TMS is occupied by a Hong Kong Observatory weather radar station. Our monitoring site was located at the waist of Mt. TMS near the mountain summit (22.405° N, 114.118° E, about 640 m a.s.l.) (see Fig. 1).

Surrounding the foot of the mountain are urban centers with a population of 2.23 million. The straight distances between the mountain summit and the urban centers at the foot are about 5–10 km. Farther to the south are the urban centers of the partial New Territory, Kowloon peninsula and Hong Kong Island. To the southwest is the newly-developed residential area of Tung Chung, the international airport and the South China Sea. To the west are the Tuen Mun residential areas and to the south is the South China Sea. To the north and northeast are the city clusters of the inland PRD region. Due to prevailing north/northeast synoptic winds in September–November, polluted air from inland PRD often reaches the sampling site. In addition, because of its unique topography, mountain-valley breezes and sea-land breezes are frequently observed at TMS. These mesoscale circulations enhance the interaction of polluted urban air and the mountain air. The sampling site was set on the rooftop of a building at the waist of TMS (22.405° N, 114.118° E; 640 m a.s.l.).

2.3 Measurement techniques

The PN concentration and size distribution, VOCs, carbonyl compounds $PM_{2.5}$, gaseous pollutants and meteorological parameters were measured in this study. The detailed information is presented as follows:

Particle size distributions in the range of 5.5 to 350 nm were continuously measured by a Scanning Mobility Particle Sizer (SMPS, model 5.400, GRIMM, Germany) and

ACPD
12, 12119–12162, 2012

a Condensation Particle Counter (CPC, model 5.400, GRIMM, Germany) system with 44 size bins at 4-min scan intervals. The SMPS was equipped with a nano-differential mobility analyzer (DMA), which separated poly-disperse particles into selected mono-disperse particles according to the electrical mobility of the particles, a function of their size. Then the CPC counted the number concentration of mono-disperse particles by laser light scattering. A sample air flow rate of $0.3\,l\,min^{-1}$ was fixed for the set of SMPS + CPC with a sheath air flow rate of $3.0\,l\,min^{-1}$. To minimize the particle loss, ambient aerosols were drawn into the SMPS+CPC system through a 1 m long flexible and conductive tube with an inner diameter of 0.8 cm. Due to significant diffusion loss of particles with size below 10 nm and diffusion broadening effect in the transfer function, it is important to understand the efficiency (or penetration rate) of the DMA for the accurate measurement of airborne particles. An experimental system determining the aerosol losses in the DMA and the calibration of the SMPS was established and discussed in Wang et al. (2012). In addition, since the Grimm CPC is not widely used, the discrepancy between Grimm CPC and TSI CPC reported by Schlatter (2006) was used to compare our results with other studies.

To understand the relationships among newly formed particles and trace gases, ambient O_3, carbon monoxide (CO), sulfur dioxide (SO_2) and nitric oxide (NO) concentrations were monitored. O_3 was measured using a commercial UV photometric instrument (Model 400E, Teledyne instrument, CA). SO_2 was measured by pulsed UV fluorescence (Model 100E, Teledyne instrument, CA). CO was measured with a gas filter correlation, non-dispersive infrared analyzer (Model 300EU, Teledyne instrument, CA) with a heated catalytic scrubber to convert CO to carbon dioxide (CO_2) for baseline determination. NO was detected with a modified commercial MoO/chemiluminescence analyzer (Model 200E, Teledyne instrument, CA). These analyzers were calibrated daily by injecting scrubbed ambient air (TEI, Model 111) and a span gas mixture. A data logger (Environmental Systems Corporation, Model 8832) was used to control the zero/span calibration and to collect 1-s data, which were averaged to 1-min values.

ACPD
12, 12119–12162, 2012

To investigate the potential associations of individual VOCs and carbonyl compounds with NPF and particle growth, non-methane hydrocarbons (NMHCs) and carbonyl samples were collected on high O_3 episode days ($O_3 \geq 100$ ppbv) i.e. on 27 October–2 November 2010, based on the prediction of meteorological conditions and the review of the PN concentrations on previous days, which were usually related to strong solar radiation, cool and dry air, and low number concentrations of pre-existing large size particles.

Ambient VOC samples were collected using cleaned and evacuated 2-l electropolished stainless steel canisters. A flow-controlling device was used to collect 1-h integrated samples. Hourly samples were consecutively collected from 09:00 to 16:00 with additional samples collected at 00:00, 03:00, 07:00, 18:00 and 21:00 per day. Finally, 91 VOC samples were collected at TMS on the seven days. The detailed analytical systems and the quality control and assurance for VOC analyses are described in Guo et al. (2009a).

Carbonyl samples were collected on the same sampling days using the silica cartridges impregnated with acidified 2,4-dinitrophenylhydrazine (DNPH). Air samples were drawn through the cartridge at a flow rate of 0.8–0.9 l min^{-1} for 120 min (2 h); the flow rate through the cartridges was monitored with a rotameter which was calibrated before and after each sampling. An O_3 scrubber was connected to the inlet of the DNPH–silica cartridge to prevent interference from O_3. During these sampling days, carbonyls samples were consecutively collected from 07:00 to 21:00 every two hours with additional samples collected at 00:00 and 03:00. Finally, 70 carbonyl samples were collected during this sampling period. All cartridges were stored in a refrigerator at 4 °C after sampling. The sampled carbonyl cartridges were eluted slowly with 2 ml of acetonitrile into a 2-ml volumetric flask. A 20-µl aliquot was injected into the high performance liquid chromatography (HPLC) system through an auto-sampler. The operating conditions of the HPLC and the quality control and detection limit for carbonyl compounds are also provided in Guo et al. (2009a).

ACPD
12, 12119–12162, 2012

Pre-fired and pre-weighed quartz fabric filters were used to collect $PM_{2.5}$ samples for 24–48 h by a high-volume sampler (1.15–1.18 $m^3\,min^{-1}$). The collected filters were weighted to determine the $PM_{2.5}$ mass using the standard gravimetric method, and then were stored in 4 °C refrigerator before chemical analysis.

To analyze inorganic ionic species in $PM_{2.5}$, i.e. ammonium (NH_4^+), sulfate (SO_4^{2-}), and nitrate (NO_3^-), sample filters were ultrasonically extracted with 10 ml of Milli-Q water for 30 min. The water extracts were filtered through a syringe filter (0.2 µm PTFE membrane) to remove filter debris and suspended insoluble particles and then stored in a bottle. The 100 µl extracts were injected into an ion chromatography (Dionex Corporation, ICS-1000) system for analysis. The detailed operations of the IC instrument are described in Wu and Wang (2007). In addition, organic carbon (OC) and elemental carbon (EC) were measured on a 0.526 cm^2 punch from each filter by thermal optical reflectance (TOR) following the IMPROVE protocol on a DRI Model 2001 thermal/optical carbon analyzer (Atmoslytic Inc., Calabasas, CA, USA) (Chow et al., 2005).

The meteorological conditions were continuously monitored using a mini-weather station (Vantage Pro TM & Vantage Pro 2 – TM Weather Stations, Davis Instruments), which consists of two components: a sleekly designed integrated sensor suite (ISS) to measure outdoor weather conditions, and a data-receiving console to receive the weather data wirelessly. The weather station was placed on the rooftop of a building at the TMS site. Temperature, relative humidity, solar radiation, UV light, wind speed and direction were recorded during the sampling period.

2.4 Data processing and analysis

2.4.1 Data processing

The first step was to divide the size distribution into 5.5–10 (nucleation mode, N_{nuc}), 10–100 (Aitken mode, N_{Ait}), and 100–350 nm (accumulation mode, N_{acc}), and to calculate

ACPD
12, 12119–12162, 2012

the total concentration of particles in each size class through the formula:

$$N_{p-q} = \alpha \sum_{p}^{q} N(\mathrm{d}p) \quad (1)$$

where N_{p-q} is the number concentration in each size class, $N(\mathrm{d}p)$ is the number concentration in the size interval $\mathrm{d}p + \Delta\mathrm{d}p$ and α is a normalization factor obtained from the equation:

$$\alpha = \log(\mathrm{d}p + \Delta\mathrm{d}p) - \log(\mathrm{d}p) \quad (2)$$

The SMPS data covered 44 channels spaced in the logarithmic scale. Calculation of the log differences between size channels in these three size modes gave an average α-value of 0.03812, 0.040202, 0.049418 for N_{nuc}, N_{Ait} and N_{acc}, respectively. The total PN concentration represented PN concentration from 5.5 to 350 nm in mobility diameter.

In this study, some data of particle size distributions from late September to early October were unavailable due to the malfunction of the DMA instrument caused by very high humidity during this period. The mean PN concentrations in different size classes were calculated with a 95 % confidence level ($p < 0.05$). The linear and power correlations between the tested parameters were indicated by a squared correlation coefficient R^2.

2.4.2 Definition of a particle formation event

In this study, nucleation events were classified into three groups (Classes Ia, Ib and II) according to the classification scheme developed by Dal Maso et al. (2005), following the criteria that the particle mode must start in the distinct nucleation mode size and the particle mode must show signs of growth with a time span of hours. Class I presents the days when the formation and growth rate are determined with a good confidence level. Class I is divided into Class Ia and Ib. The Class Ia event has clear and strong particle formation with little or no pre-existing particles, while a Class Ib

ACPD
12, 12119–12162, 2012

event is any other Class I event where the particle formation and growth rate still can be determined. A Class II event represents the event where the accuracy of formation rate calculation is questionable due to data fluctuation even though the banana shapes are still observable.

2.4.3 Calculation of formation rate, growth rate and condensational sink

In this study, particle formation rates (FR) were represented and quantified using the number concentrations of particles (5.5–10 nm) at the start and end of a linear increase period (dN_{10}/dt), without considering the effects of both coagulation and transport due to the small influence on particle production of homogenous nucleation in relatively clean air masses (Jeong et al., 2010). In this study dN_{10}/dt is a measure of the intensity of nucleation mode particle formation in the event, rather than the nucleation rate, which is typically defined as the number of nuclei clusters growing larger than 1 nm.

The observed growth rate (GR) of the newly formed particles was quantified by the evolution of geometric mean diameters (GMD) of particles from the start to the end of the particle formation events: GMD for each size distribution was used to examine particle growth processes (Dal Maso et al., 2005):

$$\mathrm{GR} = \frac{\Delta \mathrm{GMD}}{\Delta t} \tag{3}$$

The condensation sink (CS) of newly formed particles, presented as the loss rate of molecules onto existing particles, was estimated by integrating over the aerosol size distribution as follows (Kulmala et al., 2005):

$$\mathrm{CS} = 2\pi D \int D_p \beta_M(D_p) n(D_p) \mathrm{d}D_p = 2\pi D \sum_i \beta_{Mi} D_{pi} N_i \tag{4}$$

where D is the diffusion coefficient of the condensing vapor, β_M is the transitional regime correction factor, D_{pi} is the particle diameter in size class i, and N_i is the PN concentration in the respective size class.

ACPD
12, 12119–12162, 2012

3 Results and discussion

3.1 Overview of meteorological conditions and major pollutants

3.1.1 Day-to-day variations

Figures S1–S3 show the temporal variations of PN concentration (5.5–350 nm), trace gases (SO_2, NO, CO and O_3) and meteorological conditions (UV, T, RH and wind) at the TMS site in September, October and November 2010, respectively. In general, the PN concentration was the highest in November and the lowest in September, consistent with O_3 mixing ratio. The increase in PN concentration was often associated with elevated CO, NO, SO_2 and O_3 (see Figs. S1–S3), such as on 8–9 and 16–21 September, 23–24 and 27–31 October, 1–3, 8–12, 17–19 and 26–27 November, 2010. These fine particle increase events were probably attributed to primary emissions from local sources and regional transport, and secondary formation via chemical reactions.

During the sampling period, September is the wettest month in 2010 (RH: 91.2 ± 1.3 %, mean ± 95 % C.I.) and the hottest month among these three months (23.8 ± 0.5 °C). More than half of the rainfall was attributed to the two tropical cyclones, namely Lionrock and Fanapi. At the beginning of the sampling campaign, the weather in Hong Kong was fine and very hot on 6 and 7 September owing to the subsiding air associated with severe tropical storm Lionrock. On 15 September, Fanapi was formed over the Western North Pacific to the east of the Luzon Strait. Due to the subsiding air ahead of Fanapi, local weather was generally fine and hot from 16 to 19 September. At the last week of September, the northeast monsoon brought generally fine condition to Hong Kong. Affected by the tropical cyclones and northeast monsoon, the PN concentration and SO_2, CO, O_3 mixing ratio increased on 8–9 September and 16–21 September, likely associated with primary emissions and regional transport (see Fig. S1).

The mean temperature and relative humidity in October 2010 were lower than in previous years, due to an intense northeast monsoon dominating over Southern China

ACPD
12, 12119–12162, 2012

during the last six days of the month. The monsoon mainly brought fine and dry weather on 23 and 24 October, and reached the South China coast on the morning of 26 October. Affected by the intense monsoon, local temperature dropped progressively to a minimum of 15.7 °C on 28 October – the lowest of the month. A clear and typical NPF and growth event occurred on 28 October (see Sect. 3.2.1). Cool and very dry conditions with occasionally strong winds on high ground persisted for the last 5 days of the month, accompanied with the events of NPF and growth observed on 27–31 October and the O_3 episode days occurred on 29–31 October (maximum O_3: 110.4 ppbv on 31 October) (see Fig. S2).

The mean temperature and relative humidity in November were the lowest (T: 17.1 ± 0.5 °C; RH: 77.7 ± 1.6 %) among the three months. A dry northeast monsoon over Southern China brought fine and dry weather to Hong Kong on the first three days of the month. An episode of NPF events was consistently observed from 1–3 November. Affected by a broad cloud band over the coastal areas of Guangdong, the weather became rainy and cooler from 4 to 6 November. It remained fine and dry from 8 to 12 November during which another episode of NPF events occurred. Dominated by the northeast monsoon, local weather was mainly fine apart from some haze between 17 and 24 November, during which an ozone episode was recorded mainly due to regional transport on 17–19 November. On 26 November, another NPF event was observed under a cool and dry weather condition, mainly caused by the reinforcement of the northeast monsoon reaching the South China coastal areas (see Fig. S3 and Sect. 3.2).

3.1.2 Diurnal variations

Meteorological conditions and gaseous pollutants

Figure 2 shows mean diurnal variations of SO_2, NO, CO, O_3 and meteorological conditions (UV, RH, T and wind) at TMS, respectively.

ACPD
12, 12119–12162, 2012

The diurnal variation of solar radiation indicated the time of sunrise (06:00 local time LT) and sunset (18:00 LT) was similar in September, October and November. Diurnal patterns of O_3 exhibited a high peak in the afternoon and relatively low concentrations at night and in the morning. The mean daily O_3 mixing ratio was the highest in November (67.4 ± 3.0 ppbv), and the lowest in September (37.7 ± 3.6 ppbv). The daily maximum O_3 mixing ratio appeared at 14:00 ~ 15:00 LT, likely due to photochemical reactions and/or regional transport. The average daily maximum O_3 mixing ratio was 70.2 ± 6.3 ppbv.

In contrast, broad peaks of SO_2 and NO were observed at 10:00 ~ 15:00 LT and at 10:00 LT, respectively, a slight delay compared to the time (08:00 ~ 09:00) of peaks usually appeared at the urban site, perhaps due to the influence of valley breeze which brought the urban primary pollutants from mountain foot to the summit. The peak NO value (5.3 ± 0.5 ppbv) at TMS was much lower than those at urban sites (Guo et al., 2009a).

Particle number concentration and size distributions

i) Mean particle number concentration

In this study, the mean total number concentration in the size range of 5.5–350 nm at the mountain site was $7.86 \pm 0.66 \times 10^3$ cm^{-3}, falling into the range of typical values ($5–25 \times 10^3$ cm^{-3}) reported for the suburban/urban sites of North America and Europe. However, the mean PN levels at TMS were lower than that at a coastal site in Hong Kong (Yao et al., 2010), and was about 50 % less than those at some rural sites in China such as Yufa (17.0×10^3 cm^{-3}) (Yue et al., 2009) and Xinken (16.3×10^3 cm^{-3}) (Liu et al., 2008), probably due to the different altitudes of sampling sites and the emission sources near the sites. In contrast, the PN level at TMS was much higher than that (2.03×10^3 cm^{-3}) at a remote background station i.e. Mt. Waliguan in Northwestern China (Kivekäs et al., 2009), mainly attributed to the prevailing northeastern

ACPD
12, 12119–12162, 2012

synoptic winds over the TMS site, which brought polluted air masses from mainland China to Hong Kong. Furthermore, the mean values for nucleation mode (N_{nuc}, 5.5–10 nm), Aitken mode (N_{Ait}, 10–100 nm), and accumulation mode (N_{acc},100–350 nm) were $1.27 \pm 0.18 \times 10^3$, $1.63 \pm 0.35 \times 10^3$, and $0.75 \pm 0.08 \times 10^3\,cm^{-3}$ in September, respectively; $0.63 \pm 0.05 \times 10^3$, $5.65 \pm 0.76 \times 10^3$, and $0.74 \pm 0.06 \times 10^3\,cm^{-3}$ in October, respectively; and $1.74 \pm 0.13 \times 10^3$, $6.06 \pm 0.85 \times 10^3$, and $1.11 \pm 0.12 \times 10^3\,cm^{-3}$ in November, respectively. The mean highest N_{nuc} ($1.74 \pm 0.13 \times 10^3\,cm^{-3}$) was observed in November, suggesting frequent nucleation-mode particle formation at the TMS site during this period.

ii) Diurnal variations of particle number concentration and size distribution

Figure 3 shows the diurnal variations of PN concentration (5.5–350 nm) in September, October and November at TMS. As illustrated, the diurnal pattern of PN concentration was different for each of the three months. In September, the PN concentration began to rise at 08:00, reached its peak at noon, and then gradually decreased. In October, the PN concentration did not show significant difference between daytime and nighttime, likely due to many rainy and cloudy days in early and middle October. The relatively higher PN concentration in October than in September was possibly caused by the O_3 episode event occurred in late October (i.e. 27–31 October). In November, the PN concentration increased at 08:00, reached the peak value at 16:00, and then decreased. The typical diurnal pattern of PN concentration in September and November i.e. maxima at noon and afternoon and minima at night and early morning, similar to that of O_3, implied that there might be photochemical formation of new particles.

To further investigate the influence of photochemical reaction on NPF at TMS, the diurnal patterns of PN concentration and size distribution on O_3 episode and non-O_3 episode days during the sampling period are drawn in Fig. 4a, b. It is noteworthy that a day with the maximum O_3 mixing ratio higher than 100 ppb was defined as an O_3 episode day, while a day with the maximum O_3 mixing ratio lower than 50 ppb was defined as a non-O_3 episode day. Significant difference in diurnal pattern was apparently

ACPD
12, 12119–12162, 2012

observed between O_3 and non-O_3 episode days (see Fig. 4a). During daytime hours (i.e. 08:00 ~ 18:00), the PN concentration on O_3 episode days was much higher than that on non-O_3 episode days. The PN concentration started to increase at 08:00 and reached a peak value at 16:00 on O_3 episode days, whereas only a low and broad peak was observed on non-O_3 episode days. The high and sharp peak at daytime on O_3 episode days was likely attributed to local and/or regional photochemical particle formation and, to a lesser extent, the effect of valley breeze which brought PN in urban area (foot of the mountain) to the sampling site (i.e. summit of the mountain). On the other hand, the low and broad peak on non-O_3 episode days was probably due to the influence of valley breeze and regional transport. Indeed, further inspection on the size distributions of PN on O_3 episode days found that there was a small peak at nucleation mode, which indicated nucleation mode particle burst occurred on O_3 episode days. Moreover, the peak diameter for the Aitken mode was 32 nm, smaller than 65 nm on non-O_3 episode days, indicating that Aitken mode particles on O_3 episode days were probably from condensational growth and coagulation of nucleation mode particles, and from primary emissions such as traffic.

3.2 Classification of new particle formation events

According to the classification scheme developed by Dal Maso et al. (2005), the typical Class Ia events occurred on 28 October, 1, 9 and 12 November, 2010 at TMS. The examples of Class Ib observed in this study included 29 October, 2, 8 and 26 November, 2010. On 27 and 30 October, 11 and 28 November, Class II events were mainly observed.

The mean growth rate for the nucleation events was calculated by the slope of GMD against time during the period of particle growth until 25 nm. By computation, the growth rates of Class I events observed at TMS were from 2.95 to 5.00 $nm\,h^{-1}$ (average 3.90 $nm\,h^{-1}$), in line with the range of new particle growth rates observed in rural/suburban locations i.e. 1–10 $nm\,h^{-1}$ (Kulmala et al., 2004a).

ACPD
12, 12119–12162, 2012

These NPF events were often associated with elevated SO_2 and O_3. Hence, two Class Ia cases were studied to identify the sources and mechanisms that were responsible for NPF and growth in this study. Detailed description was provided as follows:

Case I – new particle formation under a clean background

New particle formation event (nucleation mode) on 28 October was clearly observed after raining on 27 October, in line with the fact that nucleation events often occur after a sharp decrease in concentrations of pre-existing particles with large surface area. The minimum temperature of 12.5 °C recorded on 28 October was the lowest in October since 1988. The NFP started when wind speed increased to achieve maximum ($5.26\,m\,s^{-1}$). As shown in Fig. 5, the nucleation mode appeared in the measurement range at about 10:00 and increased substantially with an observable growth rate ($2.95\,nm\,h^{-1}$). The nucleation mode particle concentration (N_{nuc}) increased rapidly from $\sim 1.28 \times 10^3\,cm^{-3}$ to $23.5 \times 10^3\,cm^{-3}$ at noon with a formation rate of $4.11\,cm^{-3}\,s^{-1}$. The nucleation modes shifted towards Aitken modes during the afternoon until 16:00, perhaps due to the condensation growth and coagulation of the nucleation mode particles with larger particles. Since the concentration of around $0.2–1 \times 10^6\,cm^{-3}$ of sub-5-nm particles is needed to induce a growth rate of $1\,nm\,h^{-1}$ by self-coagulation (Kulmala et al., 2004b), in this event the initial nucleation mode particle concentration of below $3 \times 10^4\,cm^{-3}$ indicated that self-coagulation only made a minor contribution to the particle growth. In addition, after 14:00, the GR decreased with the condensation sink (CS) increased from $0.0186\,s^{-1}$ to $0.0377\,s^{-1}$, indicating increased large surface area particles scavenged potential condensable vapors responsible for particle growth. After 16:00, the total PN concentration decreased rapidly, perhaps due to the dilution effect and coagulation losses. Obviously synchronous increases of O_3 with increased PN concentration suggested the photochemical reaction may contribute to the particle formation. Meanwhile, simultaneously slow increase of SO_2, decrease of CO, and rise of the calculated (HYSPLIT 4) boundary layer height were observed at the start of this event (Figs. 5 and S4), indicating that these favorite conditions for NPF were likely

ACPD
12, 12119–12162, 2012

a result of breakup of the morning inversion that mixed SO_2-enriched and CO-depleted air from aloft and diluted the accumulated urban emissions (Zhang et al., 2004).

The correlations of organic aerosol precursors i.e. VOCs and carbonyls with nucleation mode PN concentrations were analyzed to preliminarily investigate the formation mechanism of the event on 28 October. The concentrations of biogenic VOC (BVOC) and anthropogenic VOC (AVOC) species, which were demonstrated to be the potential precursors of secondary organic aerosols (SOA) reached the maxima at 07:00 ~ 09:00 (i.e. BVOCs: isoprene 96 pptv, α-pinene 24 pptv, β-pinene 6 pptv, myrcene 5 pptv and limonene 329 pptv, and AVOCs: propene 510 pptv, toluene 6079 pptv, ethyltoluenes 180 pptv and triethylbenzenes 246 pptv), 1–3 h earlier than the time when the 5.5 nm nucleation mode particles were observed. It is known that the oxidation products of BVOCs and AVOCs have a potential contribution to the new aerosol formation and growth (Griffin et al., 1999; Kulmala et al., 2004a; Hatch et al., 2011); and there is a time delay before VOC turns to condensable species which promote nucleation. Hence, the correlation of hourly PN with VOC species measured an hour earlier was explored in this study. The BVOCs i.e. isoprene, α-pinene and β-pinene and the AVOCs i.e. propene, ethyltoluenes and triethylbenzenes showed stronger correlations with N_{nuc} than other VOCs species (see Table 1). Good correlations of N_{nuc} with isoprene, α- and β-pinenes, propene and aromatics suggested that BVOCs and AVOCs could contribute to the NPF event. Indeed, chamber study suggested that the possible mechanism was the oxidation of VOCs which generated condensable oxygenated VOCs (e.g., Ng et al., 2008). In the atmosphere, methacrolein (MAC) and methyl vinyl ketone (MVK) are the major intermediate products generated from isoprene oxidation. In this event MAC and MVK showed moderate linear correlations with N_{nuc} ($R^2 = 0.414$ and 0.677, respectively), suggesting that oxidation of BVOCs was a pathway to the nucleation mode particles.

Additionally, the correlation of N_{nuc} with O_3 mixing ratio ($R^2 = 0.485$) was much higher than that with SO_2 ($R^2 = 0.030$), CO ($R^2 = 0.004$) and NO ($R^2 = 0.052$) (see

ACPD
12, 12119–12162, 2012

Table 2). All the evidences above suggested that the NPF observed on 28 October was likely due to the photochemical formation via VOC oxidation processes.

Case II – new particle formation under a polluted background

Another NPF event (nucleation mode) was clearly observed on 1 November (Fig. 6). Compared to the nucleation event occurred on 28 October, the background PN concentration on 1 November before particle nucleation was higher, which might inhibit nucleation process due to high concentrations of the pre-existing large surface area particles. However, on the morning of 1 November, the winds turned to north direction with speeds from calm to light wind, and the CO levels sharply decreased at the start of this event, probably due to the rise of the boundary layer height which caused the breakup of the morning inversion and diluted the accumulated pollutants, providing a relatively clean atmosphere (Figs. 6 and S5). Consequently, with rapid increase of solar radiation intensity and temperature, the nucleation mode appeared in the observable range at about 10:00 and the nucleation mode PN concentration increased rapidly from $\sim 3.93 \times 10^3\,cm^{-3}$ to $5.47 \times 10^3\,cm^{-3}$ in two hours (growth rate: $5.0\,nm\,h^{-1}$). Same as that on 28 October, the nucleation modes shifted towards Aitken modes in the afternoon until 14:00 on 1 November, indicating the growth of nucleation mode particles into Aitken mode particles. At 14:00 ~ 18:00, the Aitken mode PN concentration remained a stable and high level. No obvious increase in N_{nuc} in these four hours might be explained by the fact that N_{nuc} were anti-correlated with aerosol surface area concentrations, i.e. lower N_{nuc} were recorded during the periods of higher aerosol surface area concentrations. This is consistent with the observations reported in other studies (Guo et al., 2008; Liu et al., 2008). It was also supported by the condensation sink in this event that increased from $0.0228\,s^{-1}$ to $0.0455\,s^{-1}$ during the condensation process, which inhibited the nanometer-scale particle nucleation causing a decreased N_{nuc} concentration from $5.47 \times 10^3\,cm^{-3}$ to $1.36 \times 10^3\,cm^{-3}$. After 18:00, the wind direction switched to the east which might bring aged air masses to the mountain summit. Different from the NPF and growth freshly formed at the site, the aged air masses

ACPD
12, 12119–12162, 2012

transported from local urban areas and/or PRD region had high number concentrations of Aitken mode and accumulation mode particles.

In this event, only isoprene and limonene showed strong correlations with N_{nuc} (see Table 1). No correlations were found between anthropogenic VOCs and N_{nuc}. Different from the event on 28 October, the concentrations of most BVOC species started to increase at 07:00 and reached the maximum concentrations at 13:00, i.e. isoprene 118 pptv, α-pinene 10 pptv, and β-pinene 6 pptv, though myrcene and limonene reached the maximum concentrations at 07:00, i.e. myrcene 6 pptv and limonene 33 pptv. The various temporal variations and correlations of different BVOCs with the N_{nuc} indicated different oxidation processes of VOCs on these two events (i.e. 28 October and 1 November). Additionally, the correlation between O_3 mixing ratio and N_{nuc} (R^2 = 0.491) was slightly higher than that of SO_2 (R^2 = 0.314), while CO (R^2 = 0.013) and NO (R^2 = 0.121) both had no obvious correlations with N_{nuc}, confirming that the nucleation mode particles observed on 1 November were likely formed during the processes of photochemical reactions (Table 2). Given that the transformation from gas-phase pollutants to nucleation mode particles requires sufficient time, there may be a delay between the measured gaseous pollutant i.e. SO_2 and nucleation mode particles. Indeed, a much better correlation between SO_2 mixing ratio and the N_{nuc} with 2-h lag was found (R^2 = 0.637), suggesting the possible involvement of H_2SO_4 vapor or/and SO_2 oxidation products in this nucleation event. Since the SO_2 background concentration in the PRD was much higher than that required in nucleation events observed in clean environments, the nucleation of sulfuric acid should be dominant in this event apart from the contributions of oxidation of BVOCs. More detailed discussion is given in Sect. 3.3.2.1.

Previous studies on new particle growth indicate that particle growth rate depends on temperature and concentrations of available condensable vapor (Kulmala et al., 2004a). It is also reported that the semi- or no-volatile oxidation products of VOCs account for more than 70 % of the materials for the particle growth, compared to H_2SO_4 condensation which only accounts for 8.8 % of the observed growth (Boy et al., 2005).

ACPD
12, 12119–12162, 2012

Moreover, Riipinen et al. (2011) found that lower-volatility SOA is able to grow into freshly nucleated particles more effectively than semi-volatile SOA. In these years, formaldehyde concentration increased dramatically in Hong Kong (Guo et al., 2009b). Although the vapor pressures of formaldehyde, acetaldehyde and acetone as major oxidation products of VOCs are too high to take part into aerosol nucleation and growth processes, in this event, a relatively strong correlation between formaldehyde and N_{nuc} ($R^2 = 0.597$) and moderate correlations of acetaldehyde and acetone with N_{nuc} suggested that these primarily emitted carbonyls or intermediate products of BVOC oxidation could be further oxidized into semi- or no-volatile compounds, contributing to the particle growth. Additionally, compared to the event on 28 October, both MAC and MVK showed weak linear correlations with N_{nuc} ($R^2 = 0.042$ for MAC and $R^2 = 0.063$ for MVK), whereas their mother species i.e. isoprene showed a good power correlation with N_{nuc} in this event, suggesting isoprene oxidation might play an important role in N_{nuc} formation and growth, and other primary emissions of MVK and MAC weakened the correlations between photochemically produced MVK/MAC and N_{nuc}. Further investigation on the relationship between MAC and MVK found that most of the data points fell within the boundaries of lines 2:1 and 4:1, confirming the impact of regional industrial emissions on the MVK to MAC ratios (Guo et al., 2012).

3.3 Characteristics of new particle formation events

3.3.1 Effect of meteorological parameters on new particle formation

To investigate the favorable weather conditions for NPF at TMS, meteorological data in the NPF events are summarized (Table 3).

Global radiation has been identified to influence NPF. In this study, the lowest mean global solar radiation intensity from 08:00 to 16:00 on a NPF day (i.e. 28 November) was 389.3 Wm^{-2}, whereas the highest level was 565.5 Wm^{-2} on 1 November. Mejía et al. (2009) observed nucleation events when the solar radiation was 46–1063 Wm^{-2} with an average value of 394 Wm^{-2}. The nucleation events occurred when

ACPD
12, 12119–12162, 2012

the solar radiation intensity was as low as 46 Wm^{-2}, indicating that the occurrence of NPF depended not only on the presence of intense sunlight but also on the properties of the present air masses (Wehner and Wiedensohler, 2003).

In this study, temperatures on the NPF days were lower (12.5 ~ 19.7 °C) than the average temperature of the whole sampling period. For example, the minimum temperature on 28 October was 12.5 °C when NPF occurred. This study also found that NPF took place at relative humidity of 55–80 %, similar to those reported by O'Dowd et al. (2002).

In the NPF events, the northeast winds were prevailing, mainly due to intense monsoon over Southern China, which brought cool and very dry weather conditions to Hong Kong. Nevertheless, wind speeds did not show any difference between NPF days and the other days.

By inspecting the start time of the NPF events occurred at TMS, it was obvious that all the NPF events were initiated at about 10:00 ~ 11:00, consistent with other studies (Stanier et al., 2004b; Guo et al., 2008; Modini et al., 2009). Stanier et al. (2004b) claimed that nucleation was typically observed starting around 09:00 EST in Pittsburgh, USA. In Eastern Australia, the NPF events usually began at 10:00 ~ 11:00 local time (Guo et al., 2008; Modini et al., 2009), except one case in which a particularly strong nucleation event began early morning (08:00), suggesting some different, or stronger precursor sources than the sources for all other nucleation events (Modini et al., 2009). In this study, the similar start time for all the NPF events indicated that the events were mainly induced and controlled by some certain sources and pathways, which were likely to be the homogeneous and/or heterogeneous nucleation of low volatile condensable gases such as sulfuric acid and some dominated organic compounds. For instance, the diurnal variations of BVOCs i.e. isoprene, α-pinene and β-pinene showed that their mixing ratios steadily increased at 07:00, reached a maximum level in early afternoon, and then gradually decreased to low levels at night, which were consistent with the diurnal pattern of N_{nuc} or with 1–2 h time lag, indicating that the BVOC and its oxidation products had a close association with N_{nuc} formation.

ACPD
12, 12119–12162, 2012

In addition, low SO_2, NO and CO mixing ratios on the NPF days revealed that clean air masses were favorable to the NPF. Moreover, high O_3 mixing ratios in these events suggested that photochemical reaction occurred during the NPF processes.

3.3.2 Potential precursors of new particle formation

Trace gases

Table 2 shows the growth rate, formation rate and condensation sink of each NPF and growth event observed at TMS, and the correlations of SO_2, CO, NO and O_3 with the N_{nuc} for each NPF event. The N_{nuc} showed a better correlation with O_3 than with SO_2, CO and NO for most events, except for the event on 26 November, 2010, suggesting that photochemical reactions of VOCs may play a key role in the NPF. In addition, the events observed on 17 October, 1 and 8 November, 2010, showed that N_{nuc} had relatively high correlations with both O_3 and SO_2 mixing ratios (two hours ahead N_{nuc}), especially on 1 November, the SO_2 even had a better correlation with N_{nuc} than with O_3. This may indicate that SO_2 made an important contribution to the NPF in the above event. Since hydroxyl radicals (OH) and H_2SO_4 vapor were not measured, we used the product of ultraviolet radiation and SO_2 (i.e. UV × SO_2) as a surrogate parameter for H_2SO_4 production (Petäjä et al., 2009). Better correlation between N_{nuc} and the value of (UV × SO_2) (a proxy for the H_2SO_4 production rate) during the nucleation events was observed, suggesting a critical role played by H_2SO_4 in the nucleation and early growth (see Table 2).

Figure 7 shows the correlation of (UV × SO_2) with condensation sink during the NPF events at TMS. It was used to predict the required H_2SO_4 production rates for nucleation and growth of particles as a function of CS, RH, and temperature (Stanier et al., 2004b). The panel of Fig. 7 was divided into 2 qualitative regions by a 45° line. The lower right region indicated more favorable conditions to nucleation than upper left region. The threshold was calculated at representative ground-level RH and temperature values. As the UV × SO_2 product increased and the condensational sink values

ACPD
12, 12119–12162, 2012

decreased, the nucleation events were likely observed. It can be seen that most of data points fell below the dividing line. Compared to the result reported by Stanier et al. (2004b), most values of UV × SO_2 in this study were higher, confirming that this mountain site was a sulfur-rich environment, providing abundant precursor to the NPF. Indeed, the data points with high N_{nuc} concentrations fell into the right side of the figure, suggesting that nucleation events occurred at high UV × SO_2. In other word, the SO_2 oxidation products may be the trigger of NPF at TMS. Moreover, the low and relatively constant condensational sink values with low temperature and relative humidity (cold and dry) were the favorable conditions for nucleation at the site.

VOCs and carbonyl compounds

Generally, oxidation of compounds with different positions of unsaturated bonds and number of carbon atoms in the molecules can result in different aerosol growth rates and SOA mass yields (Griffin et al., 1999). In this study, it was found that the BVOCs showed much stronger correlations with N_{nuc} than the AVOCs in most cases, mainly due to the higher reactivity of BVOCs against the important atmospheric oxidants OH, NO_3 and O_3 (Table 1) (e.g., Atkinson, 2000). Particularly, isoprene, α-pinene and β-pinene had a good to moderate correlation with N_{nuc} ($R^2_{isoprene}$ = 0.303–0.653, $R^2_{\alpha-pinene}$ = 0.307–0.498 and $R^2_{\beta-pinene}$ = 0.418–0.705), indicating that these species might be the major potential contributors to NPF on these events at TMS. The higher correlations of isoprene with N_{nuc} than those of α-pinene and β-pinene in most NPF events found in this study are consistent with a previous study, in which the contributions of isoprene to SOA were found to be higher than those of α- and β-pinenes (Fu and Kawamura, 2011). Occasionally, other BVOCs i.e. myrcene and limonene (i.e. $R^2_{myrcene}$ = 0.672 on 2 November and $R^2_{limonene}$ = 0.705 on 1 November), and some AVOC species i.e. xylenes and toluene also had high correlations with N_{nuc} (i.e. $R^2_{tolunene}$ = 0.732 and R^2_{xylene} = 0.567 on 30 October), indicating that the NPF was not

ACPD
12, 12119–12162, 2012

dominated by one or two BVOC species, but by a number of factors such as the mixing ratios of BVOCs, AVOCs, O_3, OH and NO_x levels, and the degree of oxidation due to the different reaction sensitivity of individual VOCs (Hallquist et al., 2009).

Additionally, it was found that the correlation coefficient R^2 for the power curves of BVOCs vs. N_{nuc} was much higher than that of their linear correlation, and the power exponent of isoprene, α-pinene and β-pinene concentrations was from 1.05 to 2.54, 0.99 to 2.23 and 1.12 to 2.31, respectively. The recent studies on SOA formation by BVOCs found that as the BVOC species were oxidized by O_3 and OH, various products with differing volatilities were formed. When these products exceeded their saturation vapor pressure, homomolecular and heteromolecular homogeneous nucleation between H_2SO_4 and organic vapors could occur with an exponent coefficient in the range of 1 to 2 (e.g., Paasonen et al., 2010). In this study, the exponents of isoprene, α-pinene and β-pinene with N_{nuc} mainly fell into the range of 1–2, suggesting that both sulfuric acid and organic vapor may play important roles on NPF at TMS.

Laaksonen et al. (2008) concluded that oxidation products of α-pinene and other monoterpenes were not only present in the freshly nucleated particles, but also determined their growth rates. In addition, increased studies focused on the potential SO_2/acidity contribution to secondary aerosol formation and growth through heterogeneous reactions in the presence of an acid catalyst (e.g., Hatch et al., 2011). Moreover, Villani et al. (2009) reported that the particle growth can be drastically influenced by some volatile compounds in a humid environment, although these organic compounds present at low concentrations. In this study, two NPF events occurred on 27 and 30 October, with the highest GR ($9.44\,nm\,h^{-1}$) and lowest GR ($1.53\,nm\,h^{-1}$), respectively, among the six NPF events were compared. The ambient air was cleaner and humidity was higher on 27 October than that on 30 October, and the correlation coefficient ratio of BVOCs to AVOCs (R^2_{BVOCs}/R^2_{AVOCs}) and $R^2_{UV\times SO_2}$ were higher on 27 October than that on 30 October, indicating that the GR on 27 October was mainly influenced by the oxidation products of BVOCs, sulfuric acid, and to a lesser extent, the ambient

ACPD
12, 12119–12162, 2012

humidity, which was related to GR by a positive linear correlation (R^2 = 0.68) for the six NPF events.

Different from the NPF event on 27 October, the GR on 30 October may be dominated by the interactions between biogenic and anthropogenic aerosol precursors. Recent evidence suggested that chemical interactions between anthropogenic and biogenic VOCs were important in the formation of secondary aerosols (e.g., Brock et al., 2003). In this study, based on strong correlations between N_{nuc} and AVOC species and moderate correlations between N_{nuc} and BVOC species, the SOA formation may be dominated by AVOCs oxidation and/or be mediated by anthropogenic pollutants on the transformation of BVOCs to SOA on 30 October, 2010. The low formation rate and growth rate may be related to the increased condensation and the coagulation sinks caused by a large number of preexisting aerosol particles, inhibiting the formation and growth of freshly nucleated particles on 30 October 2010.

Particulate matter

Further investigation on the major inorganic chemical species i.e. sulfate (SO_4^{2-}), nitrate (NO_3^-) and ammonium (NH_4^+) and OC/EC in $PM_{2.5}$ collected from 7 September to 26 November 2010 showed that the correlations between ion mass concentrations in $PM_{2.5}$ and PN concentration were weak, i.e. R^2 = 0.214 for NH_4^+, R^2 = 0.025 for NO_3^- and R^2 = 0.252 for SO_4^{2-}. Due to strong and frequent photochemical formation from 29 October to 08 November and from 22 to 27 November, 2010, new particles formed from VOC species may contribute a significant fraction to the PN concentration in the atmosphere at TMS. Consequently, the correlations between inorganic ion mass concentrations and the PN concentration were weakened. This can be further evidenced by the fact that the OC/EC ratios obtained during the NPF events were 2.16 ~ 2.53. Typically, EC is emitted from combustion sources with limited chemical transformations, while OC can be emitted from primary sources and/or generated from chemical

ACPD
12, 12119–12162, 2012

reactions among primary gaseous VOCs in the atmosphere. Therefore, The OC/EC ratios exceeding 2.0 have been used to indicate the presence of SOA (e.g., Turpin et al., 1990). The average OC/EC ratio at TMS (i.e. 2.32), indicated a certain contribution of SOAs to the increase in PN concentration.

4 Conclusions

Particle number concentrations and size distributions were measured at a suburban site near the mountain summit of TMS from September to November 2010. The overall average concentration of nucleation mode (N_{nuc}, 5.5–10 nm), Aitken mode (N_{Ait}, 10–100 nm), and accumulation mode (N_{acc},100–350 nm) were $0.65 \pm 0.05 \times 10^3\,cm^{-3}$, $4.75 \pm 0.63 \times 10^3\,cm^{-3}$ and $0.86 \pm 0.07 \times 10^3\,cm^{-3}$, respectively. The high PN concentration was likely attributed to local photochemical particle formation and/or regional transport of aged particles. The dry monsoon season begun in late October and early November created favorable conditions for NPF. The NPF events were observed on 12 out of 35 days at TMS based on the evolution of particle size distributions and PN concentrations. Back trajectory analyses suggested that particle nucleation and growth events were associated with less polluted cool and dry air from the PRD region caused by the winter monsoon.

Good to moderate correlations between O_3 and N_{nuc} were found for almost all NPF events, suggesting that NPF events were closely related to photochemical reactions. Initial inspection on the potential precursors of the NPF events at TMS revealed that N_{nuc} had good correlations with ($UV \times SO_2$) on some days i.e. 8 November, with BVOCs on other days i.e. 29 October and 2 November, with both ($UV \times SO_2$) and BVOCs on 1 November, with both BVOCs and AVOCs on 28 October, and with VOCs and ($UV \times SO_2$) on 27 October. The results suggested that SO_2 products, BVOCs and AVOCs might be the main contributors to N_{nuc}. The SO_2 products might dominate the nucleation process while the VOCs could mainly involve in the condensation growth. Further investigation on correlations between N_{nuc} and VOC species showed that

ACPD
12, 12119–12162, 2012

isoprene, α-pinene and β-pinene might be the major potential BVOCs responsible for the NPF events at the mountain site.

Supplementary material related to this article is available online at: http://www.atmos-chem-phys-discuss.net/12/12119/2012/acpd-12-12119-2012-supplement.zip.

Acknowledgements. This project is supported by the Environment and Conservation Fund (ECF) of the Hong Kong Special Administrative Region (ECF 20/2008), and the Research Grant Council (RGC) of the Hong Kong Special Administrative Region (PolyU5179/09E).

References

Alam, A., Shi, J. P., and Harrison, R. M.: Observations of new particle formation in urban air, J. Geophys. Res., 108, 4093–4107, 2003.

Asmi, E., Kivekäs, N., Kerminen, V.-M., Komppula, M., Hyvärinen, A.-P., Hatakka, J., Viisanen, Y., and Lihavainen, H.: Secondary new particle formation in Northern Finland Pallas site between the years 2000 and 2010, Atmos. Chem. Phys., 11, 12959–12972, doi:10.5194/acp-11-12959-2011, 2011.

Atkinson, R.: Atmospheric chemistry of VOCs and NO_x, Atmos. Environ., 34, 2063–2101, 2000.

Boy, M., Kulmala, M., Ruuskanen, T. M., Pihlatie, M., Reissell, A., Aalto, P. P., Keronen, P., Dal Maso, M., Hellen, H., Hakola, H., Jansson, R., Hanke, M., and Arnold, F.: Sulphuric acid closure and contribution to nucleation mode particle growth, Atmos. Chem. Phys., 5, 863–878, doi:10.5194/acp-5-863-2005, 2005.

Brock, C. A., Trainer, M., Ryerson, T. B., Neuman, J. A., Parrish, D. D., Holloway, J. S., Nicks, Jr., D. K., Frost, G. J., Hübler, G., Fehsenfeld, F. C., Wilson, J. C., Reeves, J. M., LaFeur, B. G., Hilbert, H., Atlas, E. L., Donnelly, S. G., Schauffler, S. M., Stroud, V. R., and Wiedinmyer, C.: Particle growth in urban and industrial plumes in Texas, J. Geophys. Res., 108, 4111, doi:10.1029/2002JD002746, 2003.

Cheung, H. C., Morawska, L., and Ristovski, Z. D.: Observation of new particle formation in subtropical urban environment, Atmos. Chem. Phys., 11, 3823–3833, doi:10.5194/acp-11-3823-2011, 2011.

ACPD

12, 12119–12162, 2012

Chow, J. C., Watson, J. G., Chen, L.-W. A., Paredes-Miranda, G., Chang, M.-C. O., Trimble, D., Fung, K. K., Zhang, H., and Zhen Yu, J.: Refining temperature measures in thermal/optical carbon analysis, Atmos. Chem. Phys., 5, 2961–2972, doi:10.5194/acp-5-2961-2005, 2005.

Dal Maso, M., Kulmala, M., Riipinen, I., Wagner, R., Hussein, T., Aalto, P. P., and Lehtinen, K. E. J.: Formation and growth of fresh atmospheric aerosols eight years of aerosol size distribution data from SMEAR II, Hyytiälä, Finland, Boreal Environ. Res., 10, 323–336, 2005.

Dal Maso, M., Sogacheva, L., Aalto, P. P., Riipinen, I., Komppula, M., Tunved, P., Korhonen, L., Suur-Uski, V., Hirsikko, A., Kurtén, T., Kerminen, V.-M., Lihavainen, H., Viisanen, Y., Hansson, H.-C., and Kulmala, M.: Aerosol size distribution measurements at four Nordic field stations: identification, analysis and trajectory analysis of new particle formation bursts, Tellus B, 59, 350–361, 2007.

Dunn, M. J., Jimenez, J.-L., Baumgardner, D., Castro, T., McMurry, P. H., and Smith, J. N.: Measurements of Mexico City nanoparticle size distributions: observations of new particle formation and growth, Geophys. Res. Lett., 31, L10102, doi:10.1029/2004GL019483, 2004.

Fu, P. Q. and Kawamura, K.: Diurnal variations of polar organic tracers in summer forest aerosols: a case study of a Quercus and Picea mixed forest in Hokkaido, Japan, Geochem. J., 45, 297–308, 2011.

Gao, J., Wang, T., Zhou, X. H., Wu, W. S., and Wang, W. X.: Measurement of aerosol number size distributions in the Yangtze River delta in China: Formation and growth of particles under polluted conditions, Atmos. Environ., 43, 829–836, 2009.

Gannet, H., Douglas, H. L., Galina, C., Randolph, D. B., and Christine, W.: Persistent daily new particle formation at a mountain-top location, Atmos. Environ., 45, 4111–4115, 2011.

Griffin, R. J., Cocker III, D. R., Flagan, R. C., and Seinfeld, J. H.: Organic aerosol formation from the oxidation of biogenic hydrocarbons, J. Geophys. Res., 104, 3555–3567, 1999.

Guo, H., Ding, A. J., Morawska, L., He, C. R., Ayoko, G. A., Li, Y.-S., and Hung, W.-T.: Size distribution and new particle formation in subtropical Eastern Australia, Environ. Chem., 5, 382–390, 2008.

Guo, H., Jiang, F., Cheng, H. R., Simpson, I. J., Wang, X. M., Ding, A. J., Wang, T. J., Saunders, S. M., Wang, T., Lam, S. H. M., Blake, D. R., Zhang, Y. L., and Xie, M.: Concurrent observations of air pollutants at two sites in the Pearl River Delta and the implication of regional transport, Atmos. Chem. Phys., 9, 7343–7360, doi:10.5194/acp-9-7343-2009, 2009a.

ACPD
12, 12119–12162, 2012

Guo, H., Kwok, N. H., Cheng, H. R., Lee, S. C., Hung, W. T., Li, Y. S.: Formaldehyde and volatile organic compounds in Hong Kong homes: concentrations and impact factors, Indoor Air, 19, 206–217, 2009b.

Guo, H., Ling, Z. H., Simpson, I. J., Blake, D. R., Wang, D. W.: Observations of isoprene, methacrolein (MAC) and methyl vinyl ketone (MVK) at a mountain site in Hong Kong, J. Geophys. Res., in review, 2012.

Hallquist, M., Wenger, J. C., Baltensperger, U., Rudich, Y., Simpson, D., Claeys, M., Dommen, J., Donahue, N. M., George, C., Goldstein, A. H., Hamilton, J. F., Herrmann, H., Hoffmann, T., Iinuma, Y., Jang, M., Jenkin, M. E., Jimenez, J. L., Kiendler-Scharr, A., Maenhaut, W., McFiggans, G., Mentel, Th. F., Monod, A., Prévôt, A. S. H., Seinfeld, J. H., Surratt, J. D., Szmigielski, R., and Wildt, J.: The formation, properties and impact of secondary organic aerosol: current and emerging issues, Atmos. Chem. Phys., 9, 5155–5236, doi:10.5194/acp-9-5155-2009, 2009.

Hatch, L. E., Creamean, J. M., Ault, A. P., Surratt, J. D., Chan, M. N., Seinfeld, Y., and Prather, K. A.: Measurements of isoprene-derived organosulfates in ambient aerosols by aerosol time-of-flight mass spectrometry – Part 1: single particle atmospheric observations in atlanta, Environ. Sci. Technol., 45, 5105–5111, 2011.

Jeong, C.-H., Evans, G. J., McGuire, M. L., Chang, R. Y.-W., Abbatt, J. P. D., Zeromskiene, K., Mozurkewich, M., Li, S.-M., and Leaitch, W. R.: Particle formation and growth at five rural and urban sites, Atmos. Chem. Phys., 10, 7979–7995, doi:10.5194/acp-10-7979-2010, 2010.

Kerminen, V. M., Lehtinen, K. E. J., Anttila, T., and Kulmala, M.: Dynamics of atmospheric nucleation mode particles: a timescale analysis, Tellus B, 56, 135–146, 2004.

Kerminen, V.-M., Petäjä, T., Manninen, H. E., Paasonen, P., Nieminen, T., Sipilä, M., Junninen, H., Ehn, M., Gagné, S., Laakso, L., Riipinen, I., Vehkamäki, H., Kurten, T., Ortega, I. K., Dal Maso, M., Brus, D., Hyvärinen, A., Lihavainen, H., Leppä, J., Lehtinen, K. E. J., Mirme, A., Mirme, S., Hõrrak, U., Berndt, T., Stratmann, F., Birmili, W., Wiedensohler, A., Metzger, A., Dommen, J., Baltensperger, U., Kiendler-Scharr, A., Mentel, T. F., Wildt, J., Winkler, P. M., Wagner, P. E., Petzold, A., Minikin, A., Plass-Dülmer, C., Pöschl, U., Laaksonen, A., and Kulmala, M.: Atmospheric nucleation: highlights of the EUCAARI project and future directions, Atmos. Chem. Phys., 10, 10829–10848, doi:10.5194/acp-10-10829-2010, 2010.

Kivekäs, N., Sun, J., Zhan, M., Kerminen, V.-M., Hyvärinen, A., Komppula, M., Viisanen, Y., Hong, N., Zhang, Y., Kulmala, M., Zhang, X.-C., Deli-Geer, and Lihavainen, H.: Long term

ACPD
12, 12119–12162, 2012

particle size distribution measurements at Mount Waliguan, a high-altitude site in inland China, Atmos. Chem. Phys., 9, 5461–5474, doi:10.5194/acp-9-5461-2009, 2009.
Kulmala, M., Pirjola, L., and Makela, J. M.: Stable sulphate clusters as a source of new atmospheric particles, Nature, 404, 66–69, 2000.
Kulmala, M., Vehkamaki, H., Petajda, T., Dal Maso, M., Lauri, A., Kerminen, V. M., Birmili, W., and McMurry, P. H.: Formation and growth rates of ultrafine atmospheric particles: a review of observations, J. Aerosol Sci., 35, 143–176, 2004a.
Kulmala, M., Laakso, L., Lehtinen, K. E. J., Riipinen, I., Dal Maso, M., Anttila, T., Kerminen, V.-M., Hõrrak, U., Vana, M., and Tammet, H.: Initial steps of aerosol growth, Atmos. Chem. Phys., 4, 2553–2560, doi:10.5194/acp-4-2553-2004, 2004b.
Kulmala, M., Petäjä, T., Mönkkönen, P., Koponen, I. K., Dal Maso, M., Aalto, P. P., Lehtinen, K. E. J., and Kerminen, V.-M.: On the growth of nucleation mode particles: source rates of condensable vapor in polluted and clean environments, Atmos. Chem. Phys., 5, 409–416, doi:10.5194/acp-5-409-2005, 2005.
Laaksonen, A., Kulmala, M., O'Dowd, C. D., Joutsensaari, J., Vaattovaara, P., Mikkonen, S., Lehtinen, K. E. J., Sogacheva, L., Dal Maso, M., Aalto, P., Petäjä, T., Sogachev, A., Yoon, Y. J., Lihavainen, H., Nilsson, D., Facchini, M. C., Cavalli, F., Fuzzi, S., Hoffmann, T., Arnold, F., Hanke, M., Sellegri, K., Umann, B., Junkermann, W., Coe, H., Allan, J. D., Alfarra, M. R., Worsnop, D. R., Riekkola, M.-L., Hyötyläinen, T., and Viisanen, Y.: The role of VOC oxidation products in continental new particle formation, Atmos. Chem. Phys., 8, 2657–2665, doi:10.5194/acp-8-2657-2008, 2008.
Lee, Y., Lee, H., Kim, M., Choi, C. Y., and Kim, J.: Characteristics of particle formation events in the coastal region of Korea in 2005, Atmos. Environ., 42, 3729–3739, 2008.
Liu, S., Hu, M., Wu, Z. J., Wehner, B., Wiedensohler, A., and Cheng, Y. F.: Aerosol number size distribution and new particle formation at a rural/coastal site in Pearl River Delta (PRD) of China, Atmos. Environ., 25, 6275–6283, 2008.
McMurry, P. H., Woo, K. S., Weber, R., Chen, D. R., and Pui, D. Y. H.: Philos: size distributions of 3–10 nm atmospheric particles: implications for nucleation mechanisms, T. Roy. Soc. London A, 358, 2625–2642, 2000.
McMurry, P. H., Kuang, C. A., Smith, J. N., Zhao, J., and Eisele, F.: Atmospheric New Particle Formation: Physical and Chemical Measurements, Aerosol Measurement, John Wiley & Sons, Inc., 681–695, 2011.

ACPD
12, 12119–12162, 2012

Mejía, J. F. and Morawska, L.: An investigation of nucleation events in a coastal urban environment in the Southern Hemisphere, Atmos. Chem. Phys., 9, 7877–7888, doi:10.5194/acp-9-7877-2009, 2009.
Modini, R. L., Ristovski, Z. D., Johnson, G. R., He, C., Surawski, N., Morawska, L., Suni, T., and Kulmala, M.: New particle formation and growth at a remote, sub-tropical coastal location, Atmos. Chem. Phys., 9, 7607–7621, doi:10.5194/acp-9-7607-2009, 2009.
Mohan, M. and Payra, S.: Influence of aerosol spectrum and air pollutants on fog formation in urban environment of megacity Delhi, India, Environ. Monit. Assess., 151, 265–277, 2009.
Ng, N. L., Kwan, A. J., Surratt, J. D., Chan, A. W. H., Chhabra, P. S., Sorooshian, A., Pye, H. O. T., Crounse, J. D., Wennberg, P. O., Flagan, R. C., and Seinfeld, J. H.: Secondary organic aerosol (SOA) formation from reaction of isoprene with nitrate radicals (NO_3), Atmos. Chem. Phys., 8, 4117–4140, doi:10.5194/acp-8-4117-2008, 2008.
Oberdörster, G., Oberdörster, E., and Oberdörster, J.: Nanotoxicology: an emerging discipline evolving from studies of ultrafine particles, Environ. Health Persp., 113, 823–839, 2005.
O'Dowd, C. D., Hameri, K., Makela, J. M., Vakeva, M., Aalto, P., De Leeuw, G., Kunz, G. J., Becker, E., Hansson, H.-C., Allen, A. G., Harrison, R. M., Berresheim, H., Kleefeld, C., Geever, M., Jennings, S. G., and Kulmala, M.: Coastal new particle formation: environmental conditions and aerosol physicochemical characteristics during nucleation bursts, J. Geophys. Res., 107, 8107–8124, 2002.
Paasonen, P., Nieminen, T., Asmi, E., Manninen, H. E., Petäjä, T., Plass-Dülmer, C., Flentje, H., Birmili, W., Wiedensohler, A., Hõrrak, U., Metzger, A., Hamed, A., Laaksonen, A., Facchini, M. C., Kerminen, V.-M., and Kulmala, M.: On the roles of sulphuric acid and low-volatility organic vapours in the initial steps of atmospheric new particle formation, Atmos. Chem. Phys., 10, 11223–11242, doi:10.5194/acp-10-11223-2010, 2010.
Park, J., Sakurai, H., Vollmers, K., and McMurry, P.: Aerosol size distributions measured at the South Pole during ISCAT, Atmos. Environ., 38, 5493–5500, 2004.
Petäjä, T., Mauldin, III, R. L., Kosciuch, E., McGrath, J., Nieminen, T., Paasonen, P., Boy, M., Adamov, A., Kotiaho, T., and Kulmala, M.: Sulfuric acid and OH concentrations in a boreal forest site, Atmos. Chem. Phys., 9, 7435–7448, doi:10.5194/acp-9-7435-2009, 2009.
Qian, S., Sakurai, H., and McMurry, P. H.: Characteristics of regional n ucleation events in urban East St. Louis, Atmos. Environ., 41, 4119–4127, 2007.
Riipinen, I., Pierce, J. R., Yli-Juuti, T., Nieminen, T., Häkkinen, S., Ehn, M., Junninen, H., Lehtipalo, K., Petäjä, T., Slowik, J., Chang, R., Shantz, N. C., Abbatt, J., Leaitch, W. R.,

ACPD
12, 12119–12162, 2012

Kerminen, V.-M., Worsnop, D. R., Pandis, S. N., Donahue, N. M., and Kulmala, M.: Organic condensation: a vital link connecting aerosol formation to cloud condensation nuclei (CCN) concentrations, Atmos. Chem. Phys., 11, 3865–3878, doi:10.5194/acp-11-3865-2011, 2011.
Schlatter, J.: Comparison of Grimm and TSI Condensation Particle Counters, in: 10 ETH Conference on Combustion Generated Particles, 21–23 August, 2006.
Seinfeld, J. H. and Pandis, S. N.: Atmospheric Chemistry and Physics: From Air Pollution to Climate Change, 2nd Edn., John Wiley & Sons, p. 95, 2006.
Shen, X. J., Sun, J. Y., Zhang, Y. M., Wehner, B., Nowak, A., Tuch, T., Zhang, X. C., Wang, T. T., Zhou, H. G., Zhang, X. L., Dong, F., Birmili, W., and Wiedensohler, A.: First long-term study of particle number size distributions and new particle formation events of regional aerosol in the North China Plain, Atmos. Chem. Phys., 11, 1565–1580, doi:10.5194/acp-11-1565-2011, 2011.
Shi, Q., Sakurai, H., and McMurry, P. H.: Measurement of St. Louis aerosol size distributions: observation of particle events, in: 21st Annual AAAR Conference, 7–11 October, Charlotte, North Carolina, 2002.
Stanier, C. O., Khlystov, A. Y., and Pandis, S. N.: Ambient aerosol size distributions and number concentrations measured during the Pittsburgh Air Quality Study (PAQS), Atmos. Environ., 38, 3275–3284, 2004a.
Stanier, C. O., Khlystov, A. Y., and Pandis, S. N.: Nucleation events during the Pittsburgh Air Quality Study: description and relation to key meteorological, gas phase, and aerosol parameters, Aerosol Sci. Tech., 38, 253–264, 2004b.
Turpin, B. J., Cary, R. A., and Huntzicker, J. J.: An in-situ, time-resolved analyzer for aerosol organic and elemental carbon, Aerosol Sci. Tech., 12, 161–171, 1990.
Twomey, S. A., Piepgrass, M., and Wolfe, T. L.: An assessment of the impact of pollution on global cloud albedo, Tellus B, 36, 356–366, 1984.
US Environmental Protection Agency: Air Quality Criteria for Particulate Matter, I–III, Office of Research and Development, Washington, DC, 1996.
Vehkamäki, H., Dal Maso, M., Hussein, T., Flanagan, R., Hyvärinen, A., Lauros, J., Merikanto, P., Mönkkönen, M., Pihlatie, K., Salminen, K., Sogacheva, L., Thum, T., Ruuskanen, T. M., Keronen, P., Aalto, P. P., Hari, P., Lehtinen, K. E. J., Rannik, Ű, and Kulmala, M.: Atmospheric particle formation events at Värriö measurement station in Finnish Lapland 1998–2002, Atmos. Chem. Phys., 4, 2015–2023, doi:10.5194/acp-4-2015-2004, 2004.

ACPD
12, 12119–12162, 2012

Villani, P., Sellegri, K., Monier, M., and Laj, P.: Influence of semi-volatile species on particle hygroscopic growth, Atmos. Chem. Phys. Discuss., 9, 2021–2047, doi:10.5194/acpd-9-2021-2009, 2009.
Wang, T., Guo, H., Blake, D. R., Kwok, Y. H., Simpson, I. J., and Li, Y. S.: Measurements of trace gases in the inflow of South China Sea background air and outflow of regional pollution at Tai O, Southern China, J. Atmos. Chem., 52, 295–317, 2005.
Wang, D. W., Guo, H., and Chan C. K.: Measuring ambient acidic ultrafine particles using iron nanofilm detectors: method development, Aerosol Sci. Tech., 46, 521–532, 2012.
Weber, R. J., Moore, K., Kapustin, V., Clarke, A., Mauldin, R. L., Kosciuch, E., Cantrell, C., Eisele, F., Anderson, B., and Thornhill, L.: Nucleation in the Equatorial Pacific during PEM-Tropics B: enhanced boundary layer H_2SO_4 with no particle production, J. Geophys. Res., 106, 32767–32776, 2001.
Wehner, B. and Wiedensohler, A.: Long term measurements of submicrometer urban aerosols: statistical analysis for correlations with meteorological conditions and trace gases, Atmos. Chem. Phys., 3, 867–879, doi:10.5194/acp-3-867-2003, 2003.
Woo, K. S., Chen, D. R., Pui, D. Y. H., and McMurry P. H.: Measurement of Atlanta aerosol size distributions: observations of ultrafine particle events, Aerosol Sci. Tech., 34, 75–87, 2001.
Wu, W. and Wang, T.: On the performance of a semi-continuous $PM_{2.5}$ sulphate and nitrate instrument under high loadings of particulate and sulphur dioxide, Atmos. Environ., 41, 5442–5451, 2007.
Wu, Z. J., Hu, M., Lin, P., Liu, S., Wehner, B., and Wiedensohler, A.: Particle number size distribution in the urban atmosphere of Beijing, China, Atmos. Environ., 42, 7967–7980, 2008.
Yao, X., Choi, M. Y., Lau, N. T., Arthur Lau, P. S., Chan, C. K., and Fang, M.: Growth and shrinkage of new particles in the atmosphere in Hong Kong, Aerosol Sci. Tech., 44, 639–650, 2010.
Yue, D. L., Hu, M., Wu, Z. J., Wang, Z. B., Guo, S., Wehner, B., Nowak, A., Achtert, P., Wiedensohler, A., Jung, J. S., Kim, Y. J., and Liu, S. H.: Characteristics of aerosol size distributions and new particle formation in the summer in Beijing, J. Geophys. Res., 114, D00G12, doi:10.1029/2008JD010894, 2009.
Zhang, Q., Stanier, C. O., Canagaratna, M. R., Jayne, J., Worsnop, D. R., Pandis, S. N., and Jimenez, J. L.: Insight into the chemistry of new particle formation and growth events in Pittsburg based on aerosol mass spectrometry, Environ. Sci. Technol., 38, 4797–4809, 2004.

ACPD
12, 12119–12162, 2012

Table 1. Power correlations of BVOCs, AVOCs and carbonyls with the N_{nuc} for each NPF event observed during the sampling campaign.

Date	Biogenic VOCs							Anthropogenic VOCs				Carbonyl Compounds		
	R^2 (Isoprene)	R^2 (α-Pinene)	R^2 (β-Pinene)	R^2 (Myrcene)	R^2 (Limonene)	R^2 (Propene)	R^2 (Benzene)	R^2 (Tolunene)	R^2 (Xylene*)	R^2 (Ethyl-toluene*)	R^2 (Trimethyl-benzene*)	R^2 (Form-aldehyde)	R^2 (Acet-aldehyde)	R^2 (Acetone)
Class Ia														
28 Oct 2010	0.645	0.465	0.705	0.101	0.013	0.825	0.057	0.318	0.086	0.643	0.760	0.531	0.108	0.400
1 Nov 2010	0.653	0.204	0.231	0.015	0.705	0.369	0.272	0.310	0.275	0.200	0.080	0.597	0.470	0.435
Class Ib														
29 Oct 2010	0.520	0.362	0.116	0.060	0.352	0.064	0.014	0.034	0.029	0.054	0.169	0.227	0.336	0.425
2 Nov 2010	0.754	0.498	0.423	0.672	0.195	0.052	0.044	0.016	0.019	0.056	0.105	0.673	0.609	0.640
Class II														
27 Oct 2010	0.303	0.307	0.418	0.470	0.08	0.572	0.155	0.155	0.087	0.031	0.080	0.104	0.101	0.030
30 Oct 2010	0.620	0.440	0.488	0.269	0.083	0.135	0.383	0.732	0.567	0.433	0.196	0.955	0.776	0.698

* Xylene includes *m*-xylene, *p*-xylene and *o*-xylene; Ethyltoluene includes 2-ethyltoluene, 3-ethyltoluene and 4-ethyltoluene; Trimethylbenzene includes 1,3,5-trimethylbenzene, 1,2,4-trimethylbenzene and 1,2,3-trimethylbenzene.

ACPD
12, 12119–12162, 2012

Table 2. Linear correlations of O_3, SO_2, SO_2^* (two hours lag), UV × SO_2, NO and CO with the N_{nuc} and GR, FR, CS for each NPF event observed during the sampling campaign.

Date	R^2 (O_3)	R^2 (SO_2)	R^2 (SO_2)*	R^2 (UV × SO_2)	R^2 (NO)	R^2 (CO)	Growth Rate (nmh^{-1})	Formation Rate ($cm^{-3}s^{-1}$)	Condensation Sink (s^{-1})
Class Ia									
28 Oct 2010	0.485	0.030	0.063	0.263	0.052	0.004	2.95	4.11	0.0282
1 Nov 2010	0.491	0.314	0.637	0.694	0.121	0.013	5.00	0.29	0.0342
9 Nov 2010	0.486	0.074	0.187	0.387	0.064	0.092	3.02	0.34	0.0354
12 Nov 2010	0.562	0.121	0.264	0.273	0.084	0.189	4.63	4.53	0.0234
Class Ib									
29 Oct 2010	0.386	0.052	0.153	0.267	0.042	0.064	4.00	4.32	0.0165
2 Nov 2010	0.576	0.145	0.248	0.314	0.121	0.147	2.69	0.86	0.0364
8 Nov 2010	0.764	0.354	0.589	0.613	0.007	0.165	4.52	0.42	0.0296
26 Nov 2010	0.173	0.097	0.262	0.312	0.074	0.121	2.41	3.89	0.0144
Class II									
27 Oct 2010	0.586	0.245	0.475	0.486	0.116	0.231	9.44	3.23	0.0197
30 Oct 2010	0.684	0.102	0.253	0.261	0.053	0.115	1.53	0.51	0.0398
11 Nov 2010	0.783	0.062	0.185	0.348	0.021	0.051	8.43	3.01	0.0165
28 Nov 2010	0.316	0.013	0.174	0.264	0.008	0.031	6.45	4.01	0.0069

(SO_2)* means that SO_2 mixing ratio is two hours ahead of N_{nuc}.

ACPD
12, 12119–12162, 2012

Table 3. Summary of chemical and meteorological conditions during the NPF events observed at TMS.

Date	Start Time (LT)	Mean hourly solar radiation (08:00–16:00) (Wm^{-2})	Mean temperature (°C)	Mean relative humidity (%)	Mean wind speed (ms^{-1})	Mean wind direction (°)	Mean SO_2 (ppb)	Mean O_3 (ppb)	Mean NO (ppb)	Mean CO (ppb)	Mean PN concentration (cm-3)
Class Ia											
28 Oct 2010	1000	560.8	12.5	68.5	3.0	184.0	4.3	58.0	4.3	420.5	7.0×10^3
1 Nov 2010	1015	565.5	16.0	76.8	1.0	198.6	4.8	81.6	4.1	519.7	14.1×10^3
9 Nov 2010	1035	514.5	18.0	55.0	2.0	167.8	6.2	83.5	4.2	514.6	8.6×10^3
12 Nov 2010	1030	525.4	18.5	56.3	1.1	164.9	5.1	71.8	4.2	404.2	9.4×10^3
Class Ib											
29 Oct 2010	1030	546.2	13.4	64.8	2.6	128.2	6.0	69.5	4.2	473.7	9.8×10^3
2 Nov 2010	1015	542.0	16.4	76.7	1.3	186.1	4.2	88.9	4.1	514.3	8.7×10^3
8 Nov 2010	1030	527.8	19.4	60.5	2.2	115.5	4.6	77.9	4.2	509.2	11.1×10^3
26 Nov 2010	1045	424.1	15.2	76.1	1.2	146.5	5.1	72.9	4.2	498.6	7.4×10^3
Class II											
27 Oct 2010	1100	522.5	13.5	80.1	3.4	205.2	3.9	46.1	4.3	433.9	8.9×10^3
30 Oct 2010	1045	546.0	14.1	56.6	2.8	137.8	8.0	78.4	4.1	578.5	11.7×10^3
11 Nov 2010	1100	513.0	18.8	41.4	1.1	179.4	3.7	83.0	4.2	431.4	8.7×10^3
28 Nov 2010	1100	389.3	17.2	75.6	1.9	113.7	2.7	61.8	4.1	305.6	3.5×10^3

ACPD
12, 12119–12162, 2012

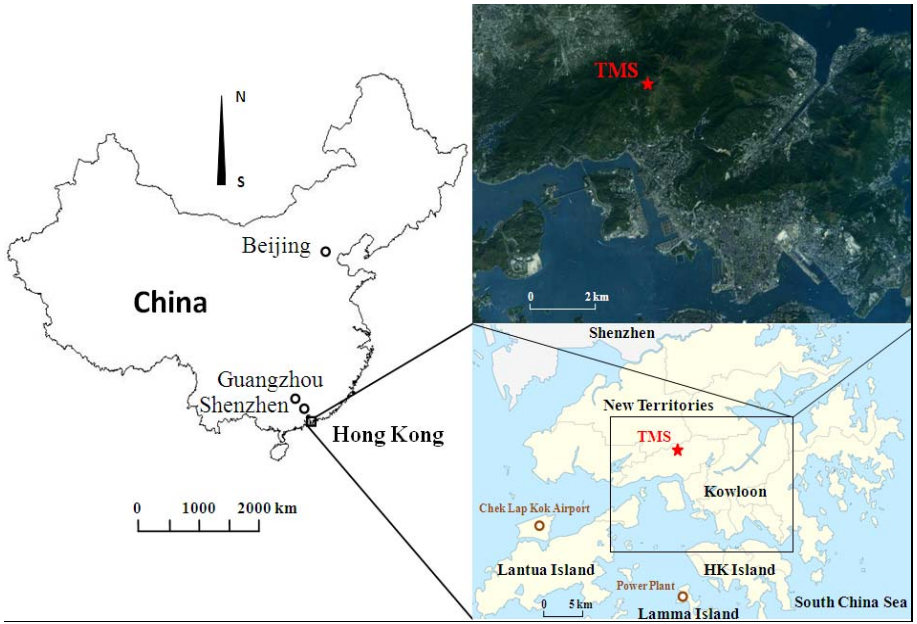

Fig. 1. Locations of Hong Kong and the TMS sampling site.

ACPD
12, 12119–12162, 2012

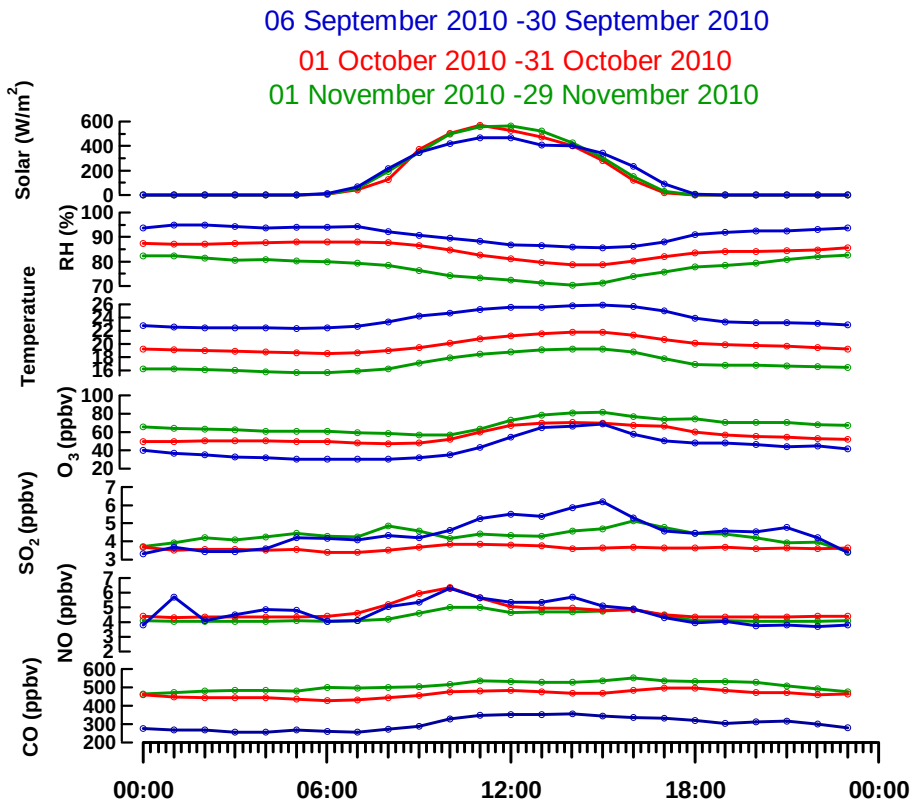

Fig. 2. Mean diurnal variations of trace gases (SO_2, NO, CO and O_3) and meteorological conditions (UV, RH, T and wind) at the TMS site in September, October and November, 2010.

ACPD
12, 12119–12162, 2012

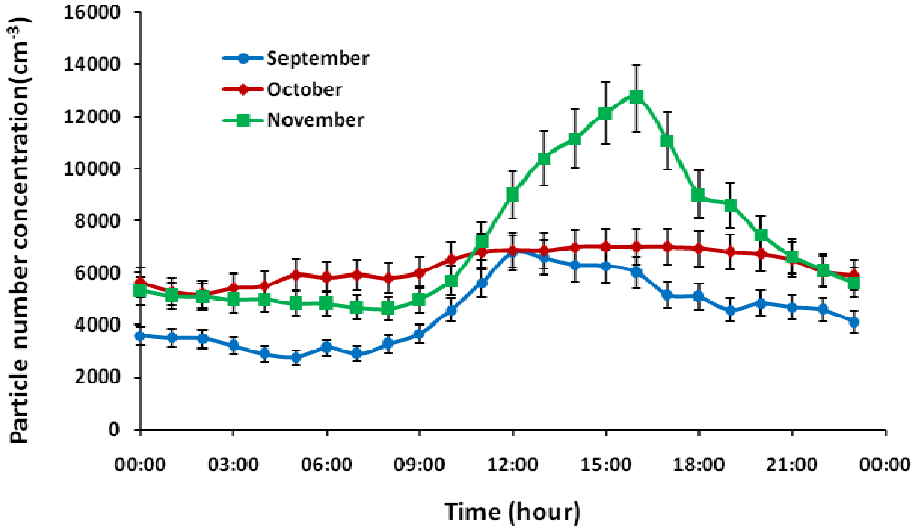

Fig. 3. Diurnal variations of PN concentration (5.5–350 nm) in September, October and November 2010 at TMS. The error bars show the standard error of the mean.

ACPD
12, 12119–12162, 2012

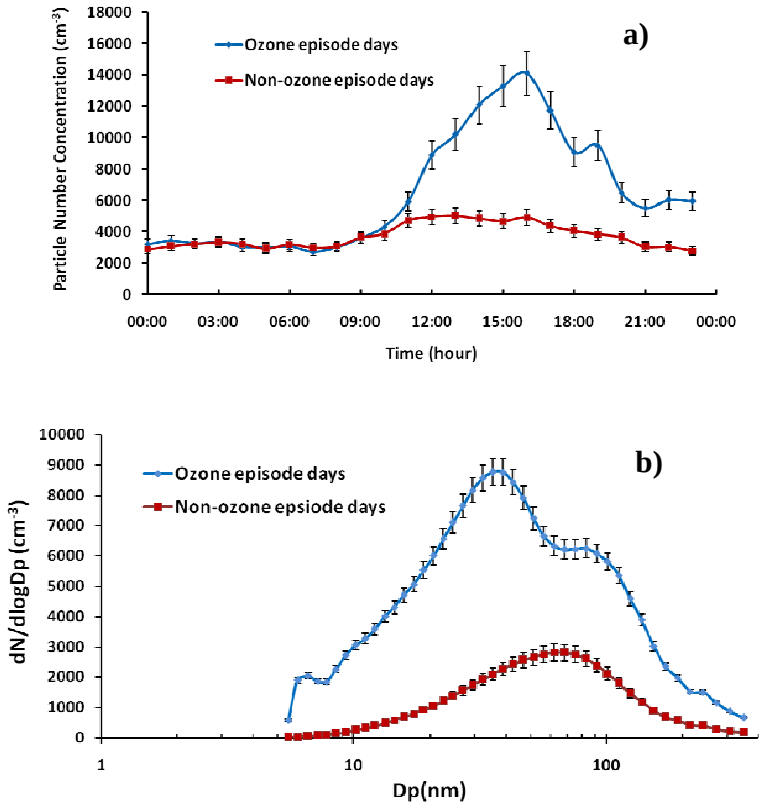

Fig. 4. Particle number concentration and size distribution on O_3 episode days (O_3 > 100 ppbv) and non-O_3 episode days (O_3 < 50 ppbv) in October and November at TMS; **(a)** diurnal variations of particle number concentration; **(b)** mean particle size distributions. The error bars show the standard error of the mean.

ACPD
12, 12119–12162, 2012

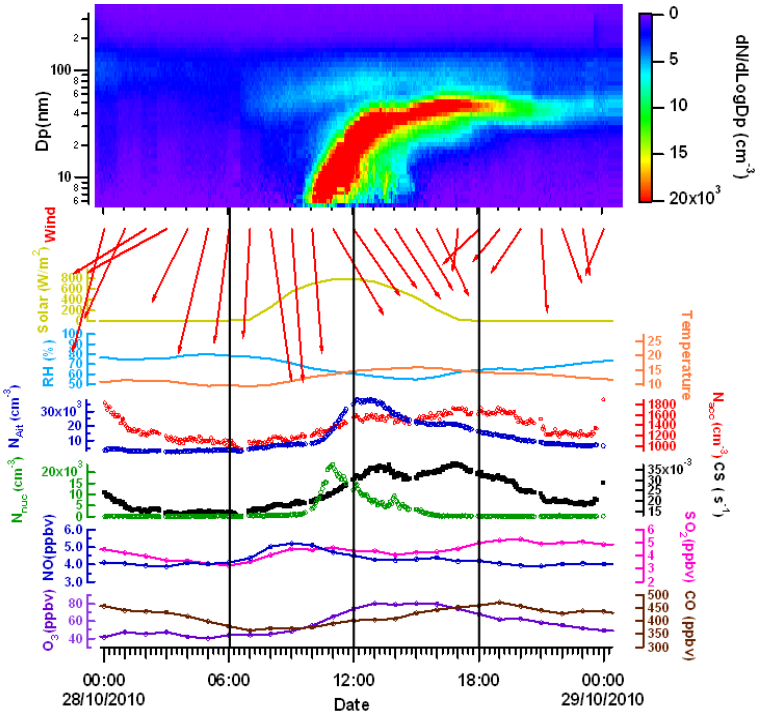

Fig. 5. Contour plots of the average diurnal variations of particle size distribution, the meteorological conditions and the concentrations of airborne pollutants on 28 October 2010 at TMS. From top to bottom, the parameters are: (i) particle size distribution; (ii) wind direction and speed (iii) solar radiation; (iv) temperature and relative humidity; (v) number concentrations of Aitken mode and accumulation mode particles; (vi) number concentration of nucleation mode particles and condensation sink, (vii) no and SO_2; (viii) O_3 and CO.

ACPD
12, 12119–12162, 2012

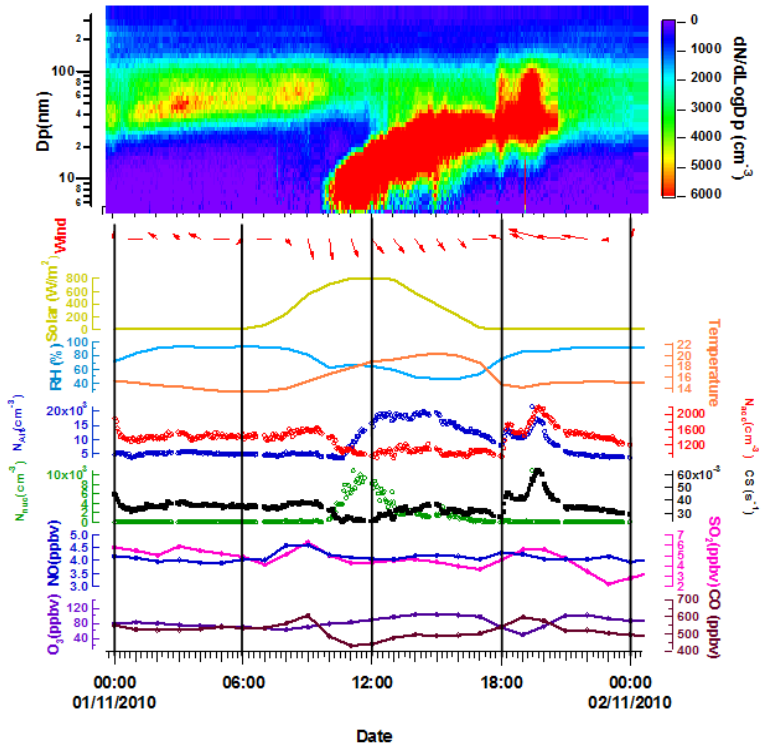

Fig. 6. Contour plots of the average diurnal variations of particle size distribution, the meteorological conditions and the concentrations of airborne pollutants on 1 November 2010 at TMS. From top to bottom, the parameters are: (i) particle size distribution; (ii) wind direction and speed (iii) solar radiation; (iv) temperature and relative humidity; (v) number concentration of Aitken mode and accumulation mode particles; (vi) number concentration of nucleation mode particles and condensation sink, (vii) NO and SO_2; (viii) O_3 and CO.

ACPD
12, 12119–12162, 2012

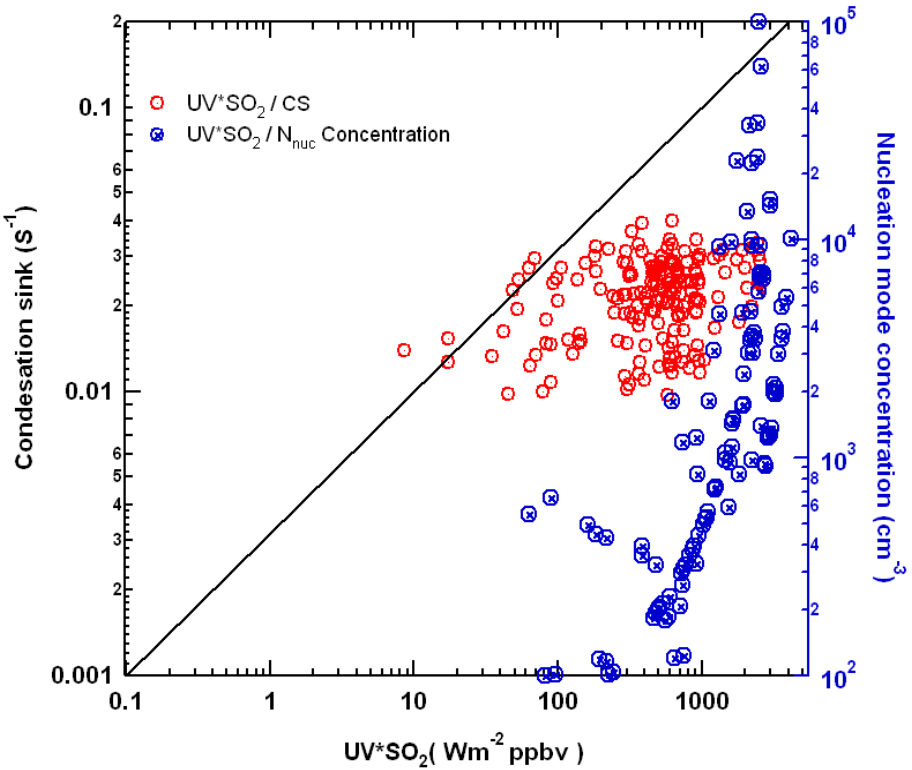

Fig. 7. Scatter plot of UV × SO_2 versus condensation sink (red dots) and UV × SO_2 versus N_{nuc} concentration (blue dots) during the NPF events. Condensational sink (y-axis – left) and nucleation mode particle concentration (y-axis – right) is plotted against the product of ultraviolet light intensity and SO_2 concentration (x-axis), respectively. Four-minute averaged values are plotted for the onset of all NPF events during this study.

ACPD
12, 12119–12162, 2012